Enhanced Cascade Sliding Mode Direct Thrust Control for Linear Induction Machine Based on Linear Metro

Abdul Khalique Junejo, *Senior Member, IEEE*, Wei Xu, *Fellow, IEEE*, Yirong Tang, *Student Member, IEEE*, Kaiju Liao, Han Xiao, and Yaohua Li, *Member, IEEE*

***Abstract*—In this article, a robust cascade sliding mode control is proposed for the direct thrust control (cascade-DTC) to achieve quicker transient response and high tracking capability with lower thrust and flux ripples for the linear induction machine (LIM). First, the fast terminal sliding mode control (FTSMC) method is designed for the speed loop to improve the speed response of LIM under DTC control structure compared to the conventional SMC (CSMC) and proportional integral control methods. Second, a supertwisting sliding mode control (ST-SMC) method is designed for both electromagnetic thrust and primary flux-linkage control loops to further improve the dynamic response in terms of transient response, steady-state response with smaller thrust and flux ripples. Third, combined speed, thrust, and flux controllers are implemented based on the FTSMC and ST-SMC for the LIM, known as the cascade-DTC technique. Afterwards, the close loop stability of the speed loop is checked by the Lyapunov function. Finally, comprehensive simulation and experimental analyses have been carried out based on one prototyped 3 kW arc induction machine to demonstrate the superiority of the cascade-DTC method than those of conventional direct thrust control, CSMC with DTC, and FTSMC based on DTC methods, respectively.**

***Index Terms*—Cascade direct thrust control (DTC) control, direct thrust control (DTC), fast terminal sliding mode control (FTSMC), linear induction machine (LIM), sliding mode control (SMC), super-twisting sliding mode control (ST-SMC).**

Manuscript received 28 December 2023; revised 9 May 2024; accepted 9 June 2024. Date of publication 17 June 2024; date of current version 16 July 2024. This work was supported in part by the National Natural Science Foundation of China under Grant 52277050, in part by the High-level Talent Program at Chinese Academy of Sciences under Grant 2Q2024000076, in part by Shenzhen International Collaboration Project under Grant GJHZ20210705142539007, and in part by Shenzhen Fundamental Research Project (General Program) under Grant JCYJ20230807143701003. Recommended for publication by Associate Editor D. Xu. *(Corresponding author: Wei Xu.)*

Abdul Khalique Junejo, Yirong Tang, Kaiju Liao, and Han Xiao are with the State Key Laboratory of Advanced Electromagnetic Technology, School of Electrical and Electronic Engineering, Huazhong University of Science and Technology, Wuhan 430074, China. (e-mail: ak.junejo@gmail.com; yirtang@hust.edu.cn; kaijuliao@hust.edu.cn; hanxiao@hust.edu.cn).

Wei Xu and Yaohua Li are with the Key Laboratory of High Density Electromagnetic Power and Systems (Chinese Academy of Sciences), Institute of Electrical Engineering, Chinese Academy of Sciences, Beijing 100190, China, and also with the University of Chinese Academy of Sciences, Beijing 101408, China. (e-mail: weixu@mail.iee.ac.cn; yhli@mail.iee.ac.cn).

Color versions of one or more figures in this article are available at https://doi.org/10.1109/TPEL.2024.3415050.

Digital Object Identifier 10.1109/TPEL.2024.3415050

Nomenclature

LIM	Linear induction machine.
RIM	Rotary induction machine.
AIM	Arc induction machine.
DTC	Direct thrust control.
PI	Proportional integral.
SMC	Sliding mode control.
Cascade-DTC	Cascade-Direct thrust control.
FTSMC	Fast terminal sliding mode control.
SVM	Space vector modulation.
ST-SMC	Supertwisting sliding mode control.

I. Introduction

THE LIM are frequently used in modern industry because of their benefits of linear motion, strong acceleration/deceleration ratio, small mechanical losses, lower noise, etc., particularly in linear metro [1], [2], [3], [4], [5]. The various control methods of RIM are very simple to design, while LIMs are difficult to implement because of their nonlinear behavior and relationship between primary and secondary, which are generally produced by the end effects (EE). The drive response of the LIMs will be degraded when speed goes up because of the EE [6], [7], [8]. Hence, robust nonlinear control methods are required to be implemented for reliable drive performance. Nowadays, DTC is getting more focus from academia and industry because of its quick dynamic performance, ease in design, insensitive to machine parameters, robust redundancy ability, etc. [9], [10], [11], [12]. However, the conventional DTC has a problem with variable switching that can be resolved by adopting the SVM method (DTC-SVM) [13]. The DTC based on SVM is better regarding the primary flux and thrust ripples under whole dynamic operation than the conventional DTC [14]. Usually, conventional PI regulators have been implemented for the speed, thrust, and primary flux loop with the DTC based on the SVM scheme, separately. Due to the overshoot, steady state error, speed fluctuation, and lower anti-disturbance ability of the PI controller in a nonlinear system [15]. Therefore, the novel control methods are required to enhance the dynamic behavior of LIMs under whole control operation. It is known from the literature survey that the flux and thrust ripples of the LIMs

are larger under PI regulators with DTC based on SVM. Since, the higher flux and thrust ripples are inadequate for the reliable control dynamics of the LIM systems. Hence, robust nonlinear control techniques are essential to the design for better control realization of the electric drive systems. The various control techniques are designed and implemented for the RIMs and LIMs to achieve smooth control operation, such as adaptive control [16], back-stepping technique [17], model predictive method [18], intelligent systems [19], SMC [20], [21], [22], [23], and so on. The SMC control method is more reliable under load disturbances and transient and steady state operation than other nonlinear methods. The SMC control method has the ability to attain quicker convergence, but it suffers from high-frequency chattering.

Recently, in [16] and [24], the SMC is used for the speed control system of the DTC-SVM method, while in [9] and [25], the SMC is designed for the current controller. These control strategies are completely examined for RIMs to decrease the sensitivity to load change. Thereof, conventional SMC is adopted to guarantee robustness and finite time convergence of the system [25], [26], [27], [28], [29]. The prominent drawback of the CSMC is slow convergence and the chattering phenomenon. These issues of the CSMC appear in the control input of the system because of the discontinuous control law and periodic switching action near the sliding surface [30].

To achieve faster transient response and high tracking ability with lower thrust and flux ripples, fast terminal sliding mode control (FTSMC) is considered for the speed controller under the SVM-DTC method for the LIM drive system. The FTSMC has the ability to achieve fast finite time convergence, stronger tracking precision, and a robust steady-state response in the whole dynamic operation. But the chattering phenomenon is still present under the FTSMC, which produces the ripples in the thrust and flux of the LIM system. To address this issue, a ST-SMC technique is designed for both electromagnetic thrust and primary flux-linkage control systems. The combined speed, thrust, and flux controllers are designed and implemented based on the FTSMC and ST-SMC for the LIM, known as the proposed cascade-DTC method. The proposed cascade-DTC has the ability to reduce thrust and flux ripples very effectively and has faster convergence, robust antidisturbance ability, and a smooth steady-state process than the CDTC, CSMC-DTC, and FTSMC-DTC, respectively. Moreover, the dynamic model of the LIM with consideration of end effects has been developed under cascade-DTC. The developed model with the cascade-DTC method can minimize the vibrations and noise problems of the LIM.

This rest of this article is organized as follows. In Section I, the appropriate literature analysis is fully reviewed. The dynamic modeling of the LIM drive system is given in Section II. The speed method based on FTSMC under the DTC strategy is designed for the LIM, as represented in Section III. In Section IV, the ST-SMC method is designed for both electromagnetic thrust and primary flux-linkage control loops. Comprehensive simulation and experimental results are presented in Sections V and VI, which fully establish that the proposed cascade-DTC can have stronger anti-disturbance ability, faster convergence speed, smaller thrust and flux ripples, and so on. Finally, Section VII concludes this article.

II. Dynamic Modeling of the LIM Drive System and Conventional DTC

The dynamic model of the LIM drive system can be obtained by adopting the synchronous reference frame. The LIM equations related to the DTC based on SVM are as follows.

The *dq*-axis voltage equations of the LIM are described as

$$u_{dq1} = R_1 i_{dq1} + p\psi_{_{dq1}} - j\omega_1 \psi_{_{dq1}} \tag{1}$$

$$u_{dq2} = R_2 i_{dq2} + p\psi_{dq2} - j\omega_{slip}\psi_{dq2} = 0 \tag{2}$$

where *1* and *2* subscripts of (1) and (2) define the primary and secondary variables under the *dq*-axis frame. The u, i, Ψ, and R are the voltage, current, flux linkage, and resistance of the LIM, individually. Furthermore, the slip speed can be defined as $\omega_{\text{slip}} = \omega_1$-$\omega_2$, where ω_1 and ω_2 are the synchronous and secondary speeds, respectively.

The flux linkage equations are illustrated as

$$\psi_{dq1} = L_1 i_{dq1} + L_{meq} i_{dq1} \tag{3}$$

$$\psi_{dq2} = L_2 i_{dq2} + L_{meq} i_{dq2} \tag{4}$$

where L_1, L_2, and L_{meq} are the primary, secondary, and magnetizing inductances of the LIM. The LIM thrust under the *dq*-axis is written as

$$F_e = (3\pi/2\tau)(\psi_{d1} i_{q1} - \psi_{q1} i_{d1}) \tag{5}$$

where τ is represents the pole pitch. Therefore, the mechanical expression of the LIM is stated as

$$F_e = F_l + (R\dot{v}_r + Tv_r)\Omega \tag{6}$$

where v_r, *R*, *T*, and Ω are the speed, total mass, the viscous friction coefficient, and compensated coefficient, respectively. Then, some parameters have been changed after the end-effect impact is taken into account in LIM, such as mutual inductance, which relies on the value of f(*Q*) that describes the average attenuation value of the flux based on the end-effect coefficient, as given by

$$f(Q) = (1 - \exp(-Q))/Q \tag{7}$$

$$Q = L_1 R_2 / L_2 v_r \tag{8}$$

where L_1 and L_2 are the primary length and secondary inductance, respectively. The modified mutual inductance is described as

$$L_{meq} = [1 - f(Q)]L_m \tag{9}$$

where L_m is the mutual inductance without end effect.

The design of the DTC-SVM can be obtained by using the primary flux linkage coordination method, where $\Psi_{d1} = \Psi_1$ and $\Psi_{q1} = 0$. The *d*-axis voltage of the LIM based on primary flux linkage can be illustrated as [9], [10], [11]

$$u_{d1} = R_1 i_{d1} + p\psi_{d1}. \tag{10}$$

The reference thrust of the LIM can be obtained by adding (1)–(5), and it is described as

$$F_e = (3\pi/2\tau R_1)\psi_1(u_{q1} - \omega_1\psi_1). \tag{11}$$

The flux and thrust of the LIM can be adjusted by the *dq*-axis voltage, as illustrated in (10) and (11).

III. Speed Control Loop Based on FTSMC Technique for the LIM

The speed controller of the LIM is designed under FTSMC with DTC (FTSMC-DTC) in this section.

A. Speed Regulation of the Speed Loop Based on Fast Terminal Sliding Mode Control (FTSMC) for LIM

The speed controller of the LIM based on FTSMC can enhance the transient response, tracking ability, and anti-disturbances capability of the LIM dive system in its whole dynamic operation. The design of the FTSMC requires state variables (speed error) for the sliding mode surface and reaching law, which are designed as follows:

$$\left.\begin{aligned}\varepsilon &= v_r^* - v_r\\ \dot{\varepsilon} &= \dot{v}_r^* - \dot{v}_r\end{aligned}\right\} \tag{12}$$

where v_r^*andv_r are the reference and actual speed of the LIM drive system, correspondingly. Then, the sliding trajectory of the FTSMC is illustrated as

$$s = \dot{\varepsilon} + k_1|\varepsilon|^{\alpha_1}\text{sign}(\varepsilon) + k_2|\varepsilon|^{\alpha 2}\text{sign}(\varepsilon). \tag{13}$$

The speed loop of the LIM based on the SMC can be developed using (13) and (14). Therefore, the input of the thrust control loop based on FTSMC is designed as follows:

$$\dot{s} = \sigma_1 s + \sigma_2\text{sign}(s). \tag{14}$$

The derivation of the actual speed can be taken from the mechanical equation of the LIM drive system, as written by

$$\dot{v}_r = B_n F_e + W_n F_l + A_n v_r \tag{15}$$

where *R* is the total mass, *T* the viscous coefficient of LIM, and A_n = -*T*/*R* and B_n = -W_n = $(\Omega R)^{-1}$ are various coefficients. Equation (6) of the LIM with load disturbance can be modified as

$$\dot{v}_r = (B_n + \Delta B)F_e + (W_n + \Delta W)F_l + (A_n + \Delta A)v_r \tag{16}$$

$$\dot{v}_r = B_n F_e + \Delta H. \tag{17}$$

Since the lumped uncertainties (ΔH) of the LIM can be illustrated as

$$\Delta H = \Delta B(F_e{}^* - F_e) + (W_n + \Delta W)F_l + (A_n + \Delta A)v_r. \tag{18}$$

By adding (17) to the derivative ε (12) then $\dot{\varepsilon}$ can be expressed as

$$\dot{\varepsilon} = \dot{v}_r^* - \dot{v}_r = \dot{v}_r^* - B_n F^*{}_e - \Delta H. \tag{19}$$

Hence, the $\dot{s}$under derivative of the speed error of the LIM drive system can be described as

$$\int \{\sigma_1 s + \sigma_2\text{sign}(s)\}\, dt = \left.\begin{aligned}&\dot{v}_r^* - B_n F^*{}_e - \Delta H\\ &+k_1|\varepsilon|^{\alpha_1}\text{sign}(\varepsilon)\\ &+k_2|\varepsilon|^{\alpha 2}\text{sign}(\varepsilon)\end{aligned}\right\}. \tag{20}$$

The thrust reference under FTSMC can be attained by simplifying (20), which is written as follows:

$$\begin{aligned}F_e{}^* &= B_n{}^{-1}(\mu_{\text{eq}} + \mu_b)\\ \mu_{\text{eq}} &= \dot{v}_r^* + k_1|\varepsilon|^{\alpha_1}\text{sign}(\varepsilon) + k_2|\varepsilon|^{\alpha 2}\text{sign}(\varepsilon) - \Delta d(t)\\ \mu_b &= \int \{\sigma_1 s + \sigma_2\text{sign}(s)\}\, dt.\end{aligned} \tag{21}$$

The bounded functions of the disturbances in the system are classified as upper and lower bounded functions, which have been derived by taking the derivative of (19)

$$\begin{aligned}\ddot{\varepsilon} &= \ddot{v}_r^* - \ddot{v}_r = \ddot{v}_r^* - B_n\dot{F}_e^* - \Delta\dot{H}\\ &= \text{E} - \Gamma\dot{F}_e^*\end{aligned} \tag{22}$$

where $E = \ddot{v}_r^* - \Delta\dot{H}$ and $\Gamma = B_n$ are the bounded variables with definite limits, which can be defined as $|\text{E}| \le \rho\, 0 < \partial_{\min} \le \Gamma \le \partial_{\max}$. The $\gamma_1$and $\gamma_2$are developed to enhance the convergence and stability of the LIM. The $\gamma_1$and $\gamma_2$are described as follows:

$$\begin{aligned}&\gamma_2 > \rho/\partial_{\min}\\ &\gamma_1 = 4\rho/\partial^2{}_{\min}\,\{\partial_{\max}(\gamma_2 + \rho)/\partial_{\min}(\gamma_2 + \rho)\}\end{aligned} \tag{23}$$

where ρ,$\partial_{\min}$, and $\partial_{\max}$are the bounded limits.

B. Stability Check

Assumption 1: The ΔH is the disturbance of (16), and by taking the derivative of the $\Delta\dot{H}$, the derivative of the $\Delta\dot{H}$ is bounded, and there is a gain $\xi h > 0$ that holds true, For every *t* $\ge$ 0. The system error will converge to zero in finite time when the system (16) meets assumption 1. But it is important that the $\sigma_2$switching gain of the reaching law satisfy $\sigma_2 > \xi_h$. The Lyapunov theorem is designated to check the stability of the close-loop system.

Therefore, the sliding mode trajectory of the FTSMC is demonstrated as

$$s = \dot{v}_r^* - B_n F^*{}_e - \Delta\dot{H} + k_1|\varepsilon|^{\alpha_1}\text{sign}(\varepsilon) + k_2|\varepsilon|^{\alpha 2}\text{sign}(\varepsilon). \tag{24}$$

Substituting (24) into (22), the sliding mode surface is gained as

$$s = \dot{v}_r^* - B_n[B_n{}^{-1}(\mu_{eq} + \mu_b)] - \Delta\dot{H}. \tag{25}$$

Also, (25) can be revised as

$$s = -\mu_b - \Delta\dot{H}. \tag{26}$$

Equation (26) can be modified by using the Lyapunov stability function as

$$\begin{aligned}\dot{s} &= -\dot{\mu}_b - \Delta\dot{H} \\ &= -\sigma_1 s - \sigma_2 \text{sign}(s) - \Delta\dot{H}. \end{aligned} \tag{27}$$

Then, the $\dot{s}s$ condition is revised as

$$\dot{s}s = -\sigma_1 s^2 - \sigma_2 s - s\Delta\dot{H}. \tag{28}$$

It can be obtained by applying the Lyapunov function to

$$\begin{aligned}\nu(x) &= \frac{1}{2}s^2 \\ \dot{V} &= s\dot{s} \\ &= -\sigma_1 s^2 - \sigma_2 |s| - s\Delta\dot{H} \\ &\le -\sigma_1 s^2 - \sigma_2 |s| - \Delta\dot{H}s \\ &- \sigma_1 s^2 - \left[\sigma_2 - \Delta\dot{H}\right]|s| \\ &\le -\sigma_1 s^2 - [\sigma_2 - \xi_h]|s| \\ &= -2\sigma_1 V - \sqrt{2}(\sigma_2 - \xi_d)V^{\frac{1}{2}}. \end{aligned} \tag{29}$$

From the above inequality, it can be proved that if $\sigma_2 > \xi_h$ the speed error will arrive at the sliding mode trajectory $s = 0$ in finite time. All switching gains are obtained by adopting the trial-and-error method so as to get better convergence, quicker tracking, and stronger robustness against load disturbances.

IV. Flux and Thrust Controllers Based on Super-Twisting Algorithm for the LIM

This section provides a detailed explanation of the design process for the thrust and primary flux linkage based on ST-SMC.

A. Thrust and Primary Flux Dynamics Under DTC Method

The primary *d*-axis voltage of the LIM under DTC-SVM control technique can be obtained through flux orientation method, i.e., $\psi_{d1} = \psi_1$and $\psi_{q1} = 0$. Hence u_{d1} is achieved by the primary *d*-axis voltage equation as follows [33]:

$$u_{d1} = R_1 i_{d1} + \rho\psi_{d_1}. \tag{30}$$

Also, the thrust of the LIM is written as

$$F_e = (3\pi/2\tau R_1)\psi_1(u_{q1} - \omega_1\psi_1). \tag{31}$$

It can be said from (30) and (31) that the primary flux and thrust of the LIM can be regulated by the *d*-axis and *q*-axis primary voltages, correspondingly.

B. ST-SMC for Thrust and Primary Flux

The primary flux and thrust errors of the LIM in state space are represented as

$$\begin{cases} x = [e_d e_q]^T = [|\psi_1^*| - |\psi_1|\ F_e^* - F_e] \\ u = [u_{d1} u_{q1}]^T \end{cases} \tag{32}$$

where e_d and e_q are the state variables for the ST-SMC and u_{d1} and u_{q1} are the inputs for the LIM. The sliding mode surface of the ST-SMC is taken as the error of the thrust (e_q) and primary flux (e_d) of the LIM. The dynamic equation for the primary flux based on ST-SMC can be defined as

$$\begin{aligned} u_{d1} &= \lambda_1 |e_d|^{\delta}\text{sign}(e_d) + N_d \\ \dot{N}_d &= -\eta_1 s - \eta_2 \text{sign}(e_d) \end{aligned} \tag{33}$$

where λ_1,η_1, and η_2 are the positive gain values of the ST-SMC and the value of the δ is selected as 0.5 which is the best value for the design and implementation on various control method [34].

Moreover, the input dynamics of primary flux loop under ST-SMC is realized by adopting the *d*-axis voltage, which is described as

$$\dot{e}_d = -\lambda_1 |e_d|^{\delta}\text{sign}(e_d) + R_1 i_{d1} - N_d. \tag{34}$$

The primary flux loop under ST-SMC for LIM is designed in (32) and $R_1 i_{d1}$ feed-forward term can be compensated by N_d effectively. Furthermore, the thrust loop controller can be designed under ST-SMC method in the similar way

$$\begin{aligned} u_{q1} &= \lambda_1 |e_q|^{\delta}\text{sign}(e_q) + N_q \\ \dot{N}_q &= -\eta_1 s - \eta_2 \text{sign}(e_q) \end{aligned} \tag{35}$$

where λ_1,η_1, and η_2 are the positive gain values of the ST-SMC. The thrust error dynamics of the LIM for ST-SMC can be obtained through the derivation of (31), as written by

$$\dot{e}_q = \kappa\dot{i}_q = -\mu\lambda_1 |e_q|^{\delta}\text{sign}(e_q) - \mu N_d + \mathrm{E} \tag{36}$$

where $\kappa = 3\pi\psi_{d1}/2\pi$, μ=$3\pi\psi_1/2\pi L_1\delta$and N_d is the disturbances of the system. The reliable and safe operation of the LIM under ST-SMC would be happened when N_d is equivalent to the E. Hence, the u_{d1}^* and u_{q1}^*under the ST-SMC for the LIM can be described as follows:

$$\begin{bmatrix} u_{d1}^* \\ u_{q1}^* \end{bmatrix} = \begin{bmatrix} \lambda_1 |e_d|^{\delta}\text{sign}(e_d) + \int \eta_1 s + \eta_2 \text{sign}(e_d) \\ \lambda_1 |e_q|^{\delta}\text{sign}(e_q) + \int \eta_1 s + \eta_2 \text{sign}(e_q) \end{bmatrix}. \tag{37}$$

The chattering phenomenon in the SMC appears due to the *sign* function. Therefore, the *sign* function can be changed to the boundary layer function, which can be written as

$$\text{sign}(s_g) = \begin{cases} 1 & \text{if}(s_g > \vartheta) \\ \frac{s_g}{\vartheta} & \text{if}(|s_g| \le \vartheta) \\ -1 & \text{if}(s_g < -\vartheta) \end{cases} \tag{38}$$

where ϑ is a small gain and the subscript *g* represents the *dq*-axis errors of the flux and thrust loop of the LIM, respectively. Moreover, to reduce chattering in the drive system, the sign function can be further modified as

$$\text{sat}(s_g) = \frac{s_g}{s_g + \vartheta}. \tag{39}$$

Hence, the modified flux and thrust loop under the sat function for ST-SMC can be described as

$$\begin{bmatrix} u_{d1}^* \\ u_{q1}^* \end{bmatrix} = \begin{bmatrix} \lambda_1 |e_d|^{\delta}\text{sat}(e_d) + \int \eta_1 s + \eta_2 \text{sat}(e_d) \\ \lambda_1 |e_q|^{\delta}\text{sat}(e_q) + \int \eta_1 s + \eta_2 \text{sat}(e_q) \end{bmatrix}. \tag{40}$$

Fig. 1 shows the overall structure of the LIM drive systems based on proposed method and Fig. 2 displays the speed controller of the LIM based on FTSMC, respectively. The whole

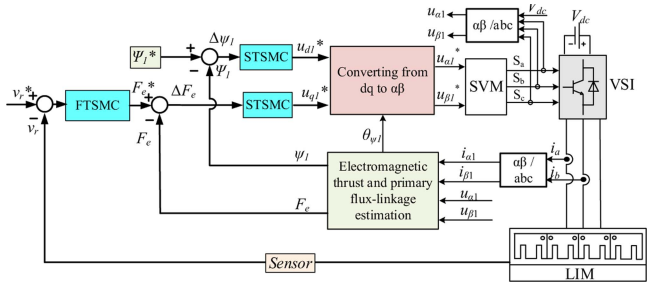

Fig. 1. FTSMC-based DTC (FTSMC-DTC) method for the LIM.

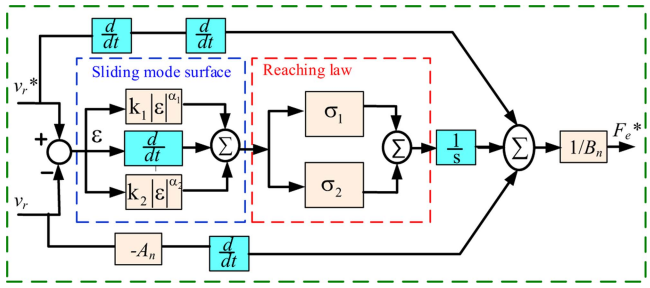

Fig. 2. FTSMC-based speed controller structure of the LIM.

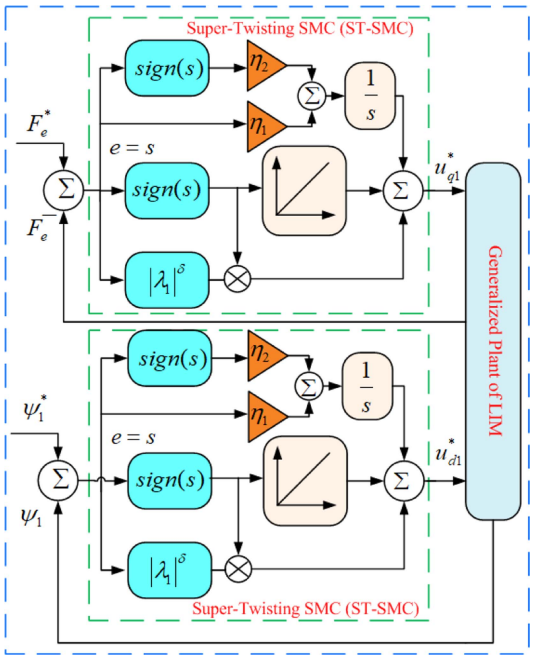

Fig. 3. ST-SMC-based thrust and speed controller for the reference voltage of LIM system.

control structure of the ST-SMC for thrust and primary flux is shown in Fig. 3. The actual thrust can be obtained by (5), and the primary flux linkage would be calculated by the voltage model with the discrete function method, as written by

$$\left.\begin{aligned} u^*_{\alpha 1} &= R_1 i_{\alpha_1} + \frac{\psi^*_{\alpha 1} - \psi_{\alpha_1}}{T_s} \\ u^*_{\beta 1} &= R_1 i_{\beta_1} + \frac{\psi^*_{\beta 1} - \psi_{\beta 1_1}}{T_s} \end{aligned}\right\} \psi^*_1 = \sqrt{(\psi^*_{\alpha 1})^2 + (\psi^*_{\beta 1})^2} \quad (41)$$

TABLE I
MAIN PARAMETERS OF THE AIM

Quantity	Symbol	Value	Unit
Rated thrust	F_N	270	N
Rated speed	v_N	11	m/s
Rated current	I_N	22	A
Pole pitch	τ	0.1485	m
Primary length	l_s	1.3087	m
Secondary resistance	R_2	2.4	Ω
Primary leakage inductance	L_{l1}	0.09	H
Primary resistance	R_1	1.06	Ω

where T_s is the sample time. The flux and thrust errors can be regulated by the ST-SMC method to obtained the reference primary voltages for the dq-axis separately. Then these primary voltages are inverted to the $\alpha\beta$-axis coordinates with the primary flux angle. Hence, the $u^*_{\alpha 1}$ and $u^*_{\beta 1}$ voltage vectors are used by the SVPWM method to obtain the switching state for the inverter.

C. Stability Check

In this section, the close loop stability checks for the flux and thrust loops are analyzed by using the Lyapunov function ($s * \dot{s} < 0$), respectively. The close loop stability of flux and thrust loops is demonstrated as

$$\begin{aligned} \dot{V} &\leq s.\dot{s} \\ \dot{V}_1 &\leq s_{dq}\dot{s}_{dq} = s_{dq}(-\lambda_1 |s_{dq}|^{\delta} \text{sign}(s_{dq})) - N_{dq} \\ &\leq s_{dq}(-\lambda_1 |s_{dq}|^{\delta} \text{sign}(s_{dq})) - N_{dq} \\ &\leq s_{dq}(-\lambda_1 |s_{dq}|^{\delta} \text{sign}(s_{dq})) - \int (\eta_{1\,sq} + \eta_2 \text{sign}(s_{dq}))dt \\ &\leq -\lambda_1 |s_{dq}|^{\delta+1} - \int (\eta_1 s^2_{dq} + \eta_2 s_{dq})dt \\ &= -2^{\frac{\delta+1}{2}} \lambda_1 V_1^{\frac{\delta+1}{2}} - \int 2\eta_1 V_1 - \sqrt{2}\eta_2 V_1^{\frac{1}{2}}. \end{aligned} \quad (42)$$

According to (42), the stability condition of the Lyapunov is verified for both the flux and thrust loops of the LIM. Hence, the ST-SMC method is asymptotically stable, and the sliding mode surface converges to zero in a finite time.

V. SIMULATION VERIFICATION

The simulation has been conducted to check the strength of the proposed method (cascade-DTC) over conventional and existing techniques individually. The dynamic behavior of the LIM has been fully demonstrated by linear speed, thrust, primary flux linkage, and phase current based on three typical working states, separately. The main parameters of the LIM have been given in Table I.

In this article, the simulation of the LIM has been presented in three different scenarios: startup response; speed variation response with constant load; and load variation response with fixed speed. The control parameters of the speed, thrust, and flux

TABLE II
CONTROL GAIN VALUES OF THE DIFFERENT CONTROL ALGORITHMS

Name	Value and unit
CDTC gain values for the speed loop based on PI controller	350 and 0.09
CSMC-DTC gain values for the speed loop based on CSMC controller	$k_1 = 300$, $\sigma_1 = 5$,$\sigma_2 = 0.01$.
FTSMC-DTC gain values for the speed loop based on FTSMC controller	$k_1 = 300, k_2 = 20$, $\alpha_1 = 0.9$,$\alpha_2 = 0.5$, $\sigma_1 = 5$,$\sigma_2 = 0.01$.
CDTC, CSMC-DTC, and FTSMC-DTC PI gain values for the Primary flux loop.	500 and 0.8
CDTC, CSMC-DTC, and FTSMCDTC PI gain values for the thrust loop.	60 and 0.2
ST-SMC primary flux and Thrust loop gains for Cascade method	(50 and 3000) and (5 and 1000) for flux and thrust loop, respectively.

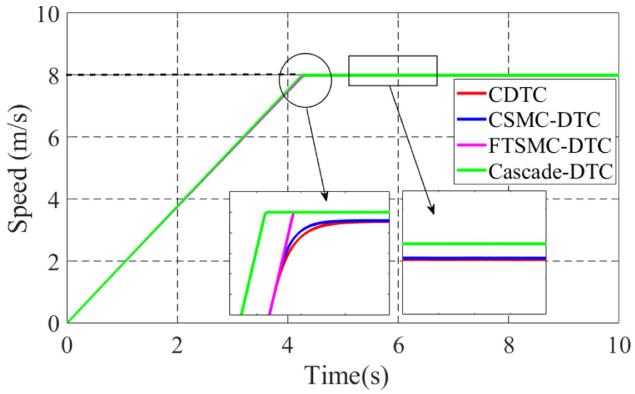

Fig. 4. Speed performance of the LIM during startup under 50 N load.

loops for the CDTC, CSMC, FTSMC-DTC, and cascade-DTC techniques are given in Table II.

A. Case 1: Start-Up and Steady-State Response

The starting response of the LIM has been fully compared among the CDTC, CSMC, FTSMC-DTC, and cascade-DTC on light load. Fig. 4 shows the linear speed response of the LIM. As seen from the same picture, the speed behavior under cascade-DTC has a quicker performance, a smaller starting transient time, and a reduced tracking error than those of CDTC, CSMC-DTC, and FTSMC-DTC, respectively. Moreover, the dynamic thrust response of the LIM has been depicted in Fig. 5, which illustrates that the cascade-DTC method has a smaller thrust rippler with faster convergence than the other three methods. Furthermore, the startup behavior of the LIM primary flux and phase current have been shown in Figs. 6 and 7 with light loads. It can be observed from Fig. 6 that the cascade-DTC method has a lesser flux ripple than CDTC, CSMC-DTC, and FTSMC-DTC individually.

It can be noted from Fig. 7 that the phase current peak amplitude under the cascade-DTC technique is less than that of the CDTC, CSMC-DTC, and FTSMC-DTC techniques. It

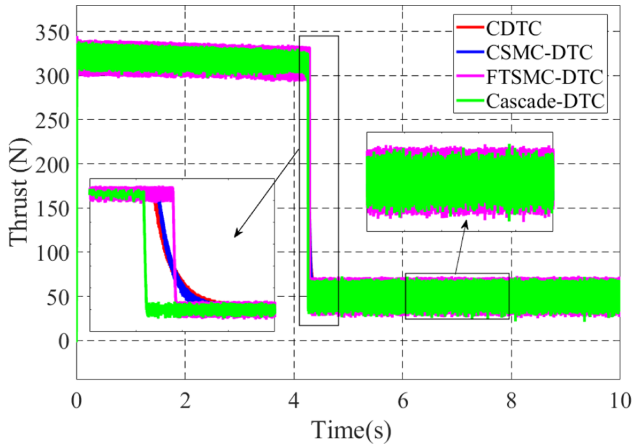

Fig. 5. Thrust behavior of the LIM during startup under 50 N load.

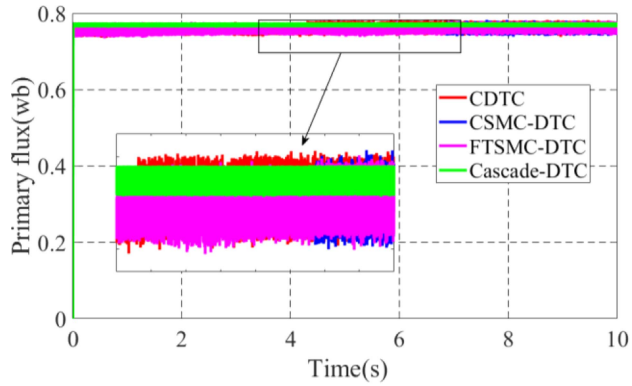

Fig. 6. Flux behavior of the LIM during startup under 50 N load.

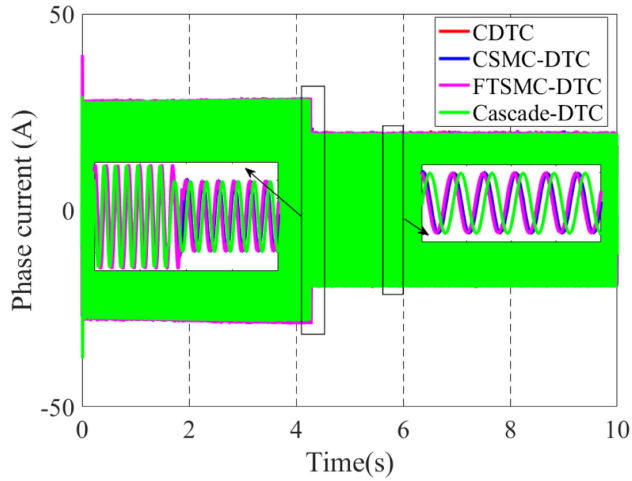

Fig. 7. Input Phase-A behavior of the LIM during startup under 50 N load.

can be concluded from the startup behavior of the LIM with CDTC, CSMC, FTSMC-DTC, and cascade-DTC that the proposed method is 7%, 6%, and 4% faster than CDTC, CSMC, and FTSMC-DTC, respectively. Likewise, the thrust response with the cascade-DTC technique is 5%, 5.3, and 7.5% smaller than the

TABLE III
THRUST AND FLUX RIPPLES FOR CDTC, CSMC-DTC, FTSMC-DTC, AND CASCADE-DTC

Control Method	Thrust ripple	Flux ripple
CDTC	32.5 %	5.2%
CSMC-DTC	34.1%	4.9%
FTSMC-DTC	28.6%	4.87%
Cascade-DTC	24%	1.3%

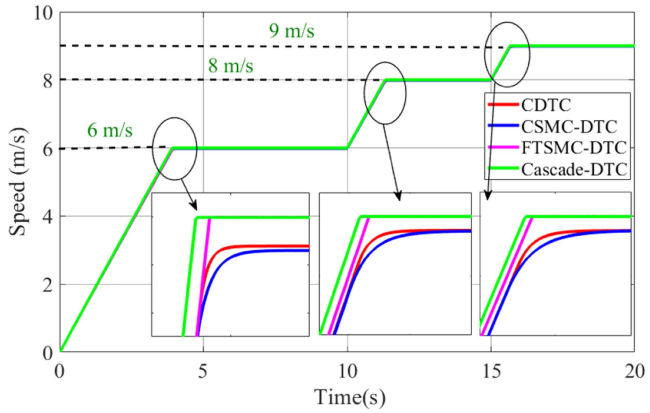

Fig. 8. Speed behavior under speed change behaviour of the LIM under 100 N load.

other three methods. Moreover, the flux ripple under cascade-DTC is significantly less than CDTC, CSMC, and FTSMC-DTC separately. The comparative analysis among the four methods for thrust and flux ripples is given in Table III. It is observed from Table III that the proposed method has advantages over the CDTC and FTSMC-DTC in terms of lower thrust and flux ripples, respectively.

B. Case 2: Speed Variation Performance of the LIM With Fixed Load

The speed change scenario has been established for the LIM drive system under CDTC, CSMC-DTC, FTSMC-DTC, and cascade-DTC with a 100 N load to verify the superiority of the cascade-DTC technique. In this test, the speed change system is applied to four control methods. The LIM has been started with a 0 to 6 m/s speed with a 100 N load, then the speed has been varied from 6 to 8 m/s at the time of 10 s, and again the speed has been changed from 8 to 9 m/s at the time of 15 s with the same load. The linear speed, thrust, flux, and phase current responses of the LIM are shown in Figs. 8, 9, 10, and 11 under the speed change scenario with constant load. It can be seen from Fig. 8 that all control methods track the reference speed during the whole dynamic speed operation. It can be seen from the same picture that the speed under the cascade-DTC method has quicker behavior with a better tracking error than CSMC-DTC and FTSMC-DTC individually.

Fig. 9 demonstrates the thrust response of the LIM under speed change conditions for four control methods. It can be noted

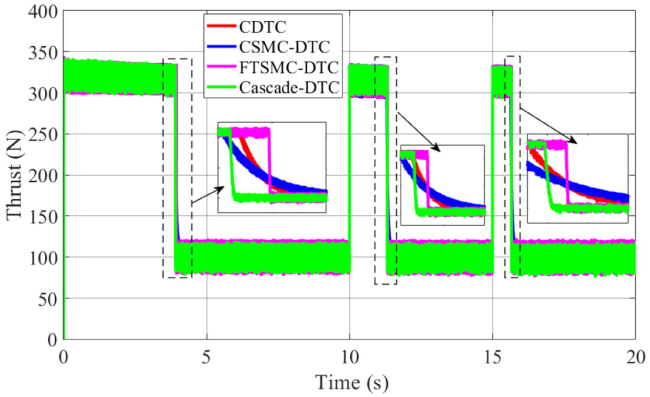

Fig. 9. Thrust behavior under speed change behaviour of the LIM under 100 N load.

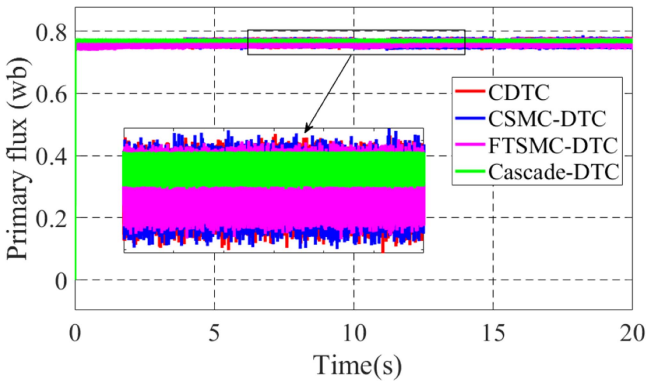

Fig. 10. Flux behavior under speed change behaviour of the LIM under 100 N load.

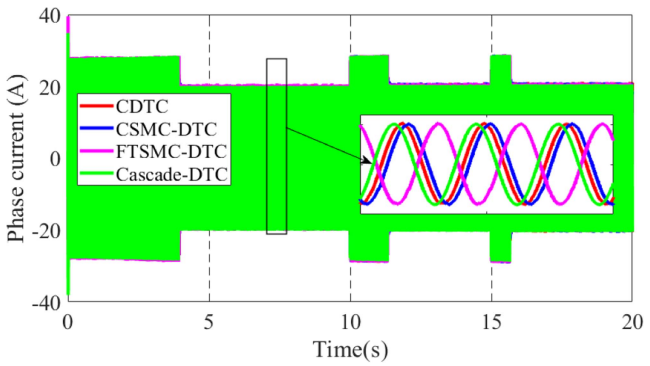

Fig. 11. Phase-A current behavior under speed change behaviour of the LIM under 100 N load.

from this picture that the thrust behavior under CDTC, CSMC-DTC, FTSMC-DTC, and cascade-DTC tracks the reference thrust with speed change. It can be further observed from Fig. 9 that the thrust ripple is smaller in the proposed technique than the three methods, correspondingly. The primary flux linkage is displayed in Fig. 10 for the four control techniques. It is obviously shown in this picture that the cascade-DTC technique has a significantly smaller flux ripple than CDTC, CSMC-DTC,

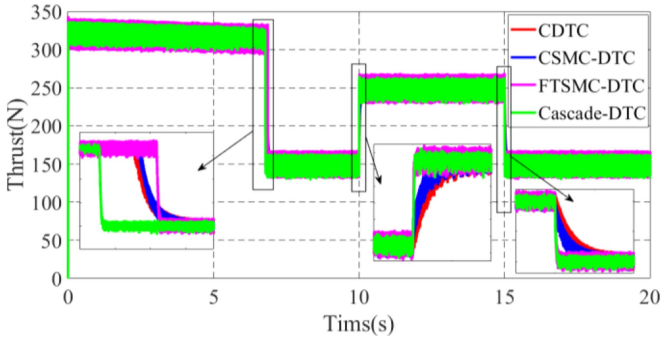

Fig. 12. Thrust behavior under load change behaviour of the LIM under 8 m/s speed.

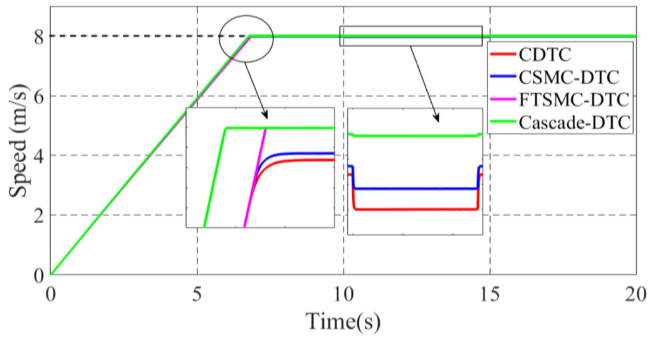

Fig. 13. Speed behavior under load change behaviour of the LIM under 8 m/s speed.

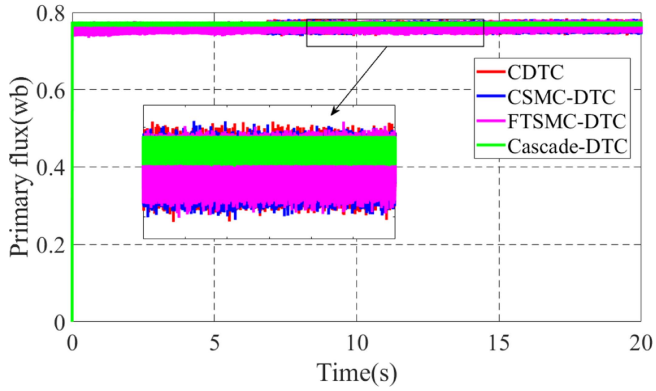

Fig. 14. Flux behavior under load change behaviour of the LIM under 8 m/s speed.

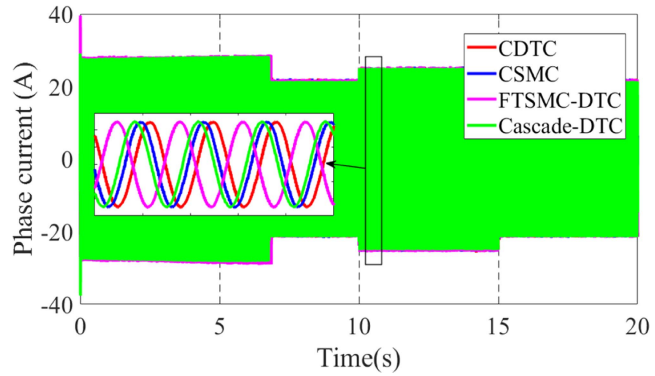

Fig. 15. Phase-A current behavior under load change behaviour of the LIM under 8 m/s speed.

and FTSMC-DTC. The Phase current of the LIM drive system for CDTC, CSMC-DTC, FTSMC-DTC, and cascade-DTC is shown in Fig. 11 for speed change conditions. The phase current is changing as speed changes, but it is observed from the same figure that the peak value of the Phase current is less with cascade-DTC than with CDTC, CSMC-DTC, and FTSMC-DTC, completely.

C. Case 3: Load Variation Response of the LIM Drive

The load change scenario has been developed for the LIM drive system under CDTC, CSMC-DTC, FTSMC-DTC, and cascade-DTC with a speed of 8 m/s to check the robustness of the cascade-DTC technique. In this test, the load change is applied to four control methods. The LIM has been started with a 150 N load at a fixed speed of 8 m/s, then the load has been varied from 150 to 250 N at the time of 10 s, and again the load has been altered from 250 to 150 N at the time of 15 s with the 8 m/s speed. The thrust, linear speed, flux, and phase current responses of the LIM are shown in Figs. 12, 13, 14, and 15 under the load change scenario with 8 m/s speed, individually. It can be seen from Fig. 12 that all control methods track the reference thrust throughout the whole dynamic operation of the LIM.

It can be observed from the same image that the thrust response under CDTC, CSMC-DTC, FTSMC-DTC, and cascade-DTC tracks the reference thrust with constant speed. It can be further realized from Fig. 12 that the thrust ripple is less in the proposed technique than the three methods, correspondingly. Fig. 13 displays the speed response under load change conditions. It can be observed from this figure that the cascade-DTC technique has quicker behavior with a better tracking error than CSMC-DTC and FTSMC-DTC, respectively. The flux response to the load change scenario is depicted in Fig. 14, which shows that the primary flux linkage has a significantly smaller flux ripple than CDTC, CSMC-DTC, and FTSMC-DTC. The phase current of the LIM under CDTC, CSMC-DTC, FTSMC-DTC, and cascade-DTC is shown in Fig. 15 for load change conditions. The phase current is changing as load changes, but it is observed from the same figure that the peak value of the phase current is less with cascade-DTC than with CDTC, CSMC-DTC, and FTSMC-DTC, finally.

VI. Experiments and Analysis

In order to check the superiority of the cascade-DTC technique, an experimental platform has been established in the laboratory, as displayed in Fig. 16. The saturation limit of the thrust loop and the control gains of the CDTC, FTSMC-DTC, and cascade-DTC are kept constant to ensure fair validation. The dc voltage has been fixed at 300 V for the CDTC, FTSMC-DTC, and cascade-DTC, and the linear speed is fixed up to 8 m/s for

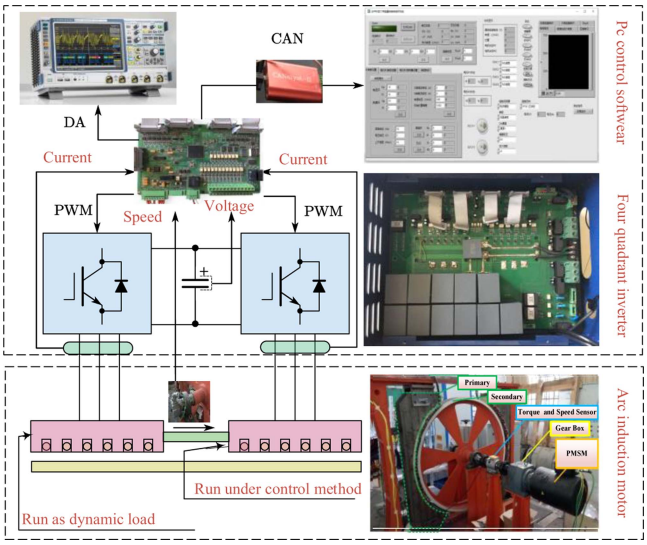

Fig. 16. Experimental platform of AIM.

TABLE IV
PERFORMANCE INVESTIGATION OF THE LIM FOR TRANSIENT TIME AND CURRENT THD UNDER CDTC, FTSMC-DTC AND CASCADE-DTC METHODS

Dynamic behaviors / Different states		CDTC	FTSMC-DTC	Cascade-DTC
Transient time (s)	Startup	5.6	3.2	3.0
	Speed variation	8.76	6.81	5.4
	Load change	10.47	5.37	3.3
Current THD	Steady State dynamics	13.34%	9.27%	8.2%

TABLE V
COMPUTATION TIME OF THE CONTROL METHODS

Control Method	Execution Time (μs)
CDTC	20
CSMC-DTC	34
FTSMC-DTC	52
Cascade-DTC	84

the reliable and safe control of the induction machine AIM. In this article, the experimental analysis of the AIM is conducted to verify the robustness of the cascade-DTC method under three different scenarios: startup performance; speed variation response with constant load; and load alteration response with constant speed. Furthermore, the startup response of the LIM primary flux and phase current have been displayed in Fig. 18(c), and (d), with 100 N thrust load. It can be observed from Fig. 19(c) that the cascade-DTC method has a smaller flux ripple than those of the CDTC, and FTSMC-DTC individually. It can be noted from Fig. 18(d) that the phase current peak amplitude under the cascade-DTC technique is smaller than that of the other three control techniques.

A. Case 1: Start-Up Response and Harmonic Analysis

The starting response with a speed of 0 to 7 m/s of the AIM has been fully compared among the CDTC, FTSMC-DTC, and cascade-DTC on the 100 N fixed load shown in Fig. 17(a), (b), and (c). Fig. 18(a) displays the dynamic linear speed of the AIM drive system. As realized from the same picture, the speed profile under cascade-DTC has a faster response and a lesser tracking error than CDTC and the same as FTSMC-DTC, respectively. It can be further noticed that the CDTC has an overshoot. It can be concluded that the speed behavior of the AIM under cascade-DTC and FTSMC-DTC has a 20% faster response than the CDTC. Moreover, the thrust performance of the AIM has been depicted in Fig. 18(b). As shown in the same image, the cascade-DTC method has a smaller thrust rippler with faster convergence than the other three methods. Besides, the harmonic analysis test has been conducted by using the fast Fourier transform on the three phase currents of the AIM during steady state conditions under Cascade-DTC, CDTC, and FTSMC-DTC, respectively. The comparative harmonic spectrum analysis of the aforementioned techniques is displayed in Fig. 19.

It can be observed from Fig. 19 that the magnitude component and total harmonic distortion (THD) of the current are smaller under the proposed method other than CDTC and FTSMC-DTC (about 5% and 1% current THD reduced) separately. The transient time and THD of cascade-DTC, FTSMC-DTC, and CDTC are given in Table IV.

Moreover, the computational burden of the CDTC, FTSMC and cascade-DTC has been checked online from the DSP board, which is shown in Fig. 20.

It can be realized from the same picture that the CDTC has lower computational burden than the FTSMC and proposed method, respectively. The computational time is given in Table V for four control methods. However, the proposed method has more robust performance than that of the CDTC and FTSMC in terms of quicker dynamic response in transient time, better steady state performance, lower thrust and flux ripples with lower THD and robust anti-disturbances property, correspondingly.

B. Case 2: Speed Variation Performance of the LIM With Fixed Load

The speed change state is established for the AIM under CDTC, FTSMC-DTC, and cascade-DTC with a 100 N load to verify the effectiveness of the proposed method. In this test, the speed change system is applied to three control methods. The AIM has been started with a 0 to 6 m/s speed with a 100 N load, then the speed has been changed from 6 to 8 m/s at the time of 35 s, and again the speed has been changed from 8 to 6 m/s at the time of 70 s with the same load. The linear speed, thrust, flux, and phase current responses of the LIM are shown in Fig. 21(a),

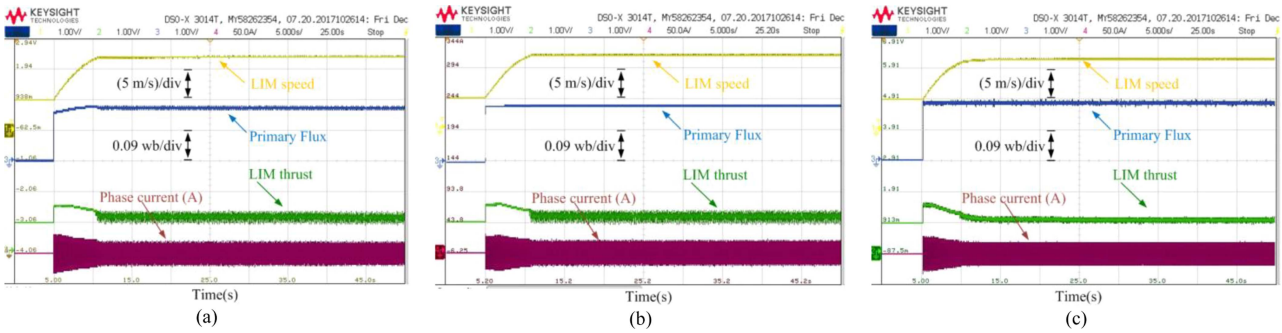

Fig. 17. The startup profiles of the AIM under 7 m/s speed with 100 N load. (a) CDTC. (b) FTSMC-DTC. (c) Cascade-DTC.

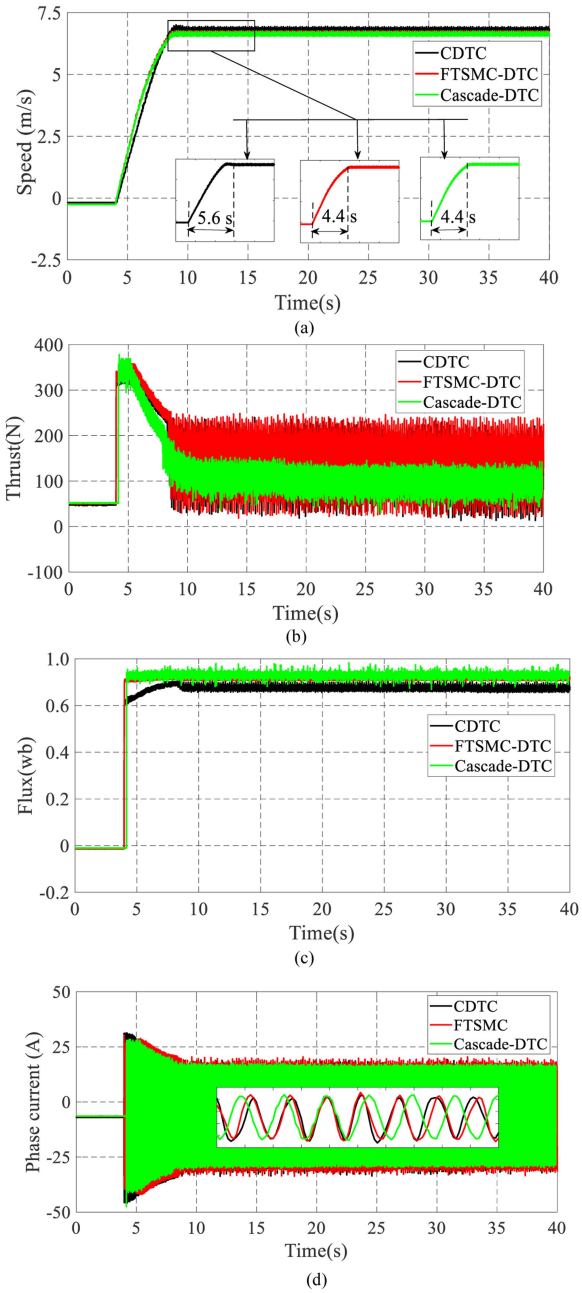

Fig. 18. Startup and steady-state performance of CDTC, FTSMC and cascade-DTC techniques under light load at 7m/s. (a) Speed. (b) Thrust. (c) Flux. (d) Phase current.

(b), and (c) under the speed change scenario with constant load, correspondingly. It can be realized from Fig. 22(a) that all control methods track the reference speed during the whole dynamic speed operation. It can be seen from the same figure that the speed under the cascade-DTC technique has a quicker response with a better tracking error than CDTC and FTSMC-DTC, respectively. Fig. 22(b) shows the thrust profile of the LIM under speed change conditions for four control methods. It can be noted from this picture that the thrust behavior under CDTC, FTSMC-DTC, and cascade-DTC tracks the reference thrust with speed change. It can be further noticed from Fig. Fig. 22(b) that the thrust ripple is lesser in the proposed method than the three methods, similarly. The primary flux linkage is displayed in Fig. Fig. 22(c) under three control methods. It is obviously shown in this picture that the cascade-DTC technique has a significantly smaller flux ripple than CDTC, and FTSMC-DTC. The Phase current of the LIM under CDTC, FTSMC-DTC, and cascade-DTC is shown in Fig. 22(d) for speed change conditions. The phase current is changing as speed changes, but it is observed from the same figure that the peak value of the Phase current is less with cascade-DTC than with CDTC, and FTSMC-DTC, completely.

C. Case 3: Load Variation Response of the AIM Drive System

The load change scenario has been developed for the AIM under CDTC, FTSMC-DTC, and cascade-DTC with a speed of 7 m/s to check the robustness of the cascade-DTC technique. In this test, the load change is applied to three control methods. The AIM has been started with a 150 N load with a fixed speed of 7 m/s, then the load has been varied from 150 to 100 N at the time of 35 s, and again the load has been altered from 100 to 150 N at the time of 70 s with the 7 m/s speed. The thrust, linear speed, flux, and phase current responses of the LIM are shown in Fig. 23(a), (b), and (c) under the load change scenario with 7 m/s speed, individually. It can be seen from Fig. 23(a), (b), and (c) that all control methods track the reference thrust throughout the whole dynamic operation of the LIM. It can be observed from the same picture that the thrust behavior under CDTC, FTSMC-DTC, and cascade-DTC tracks the reference thrust with constant speed. It can be further observed from Fig. 24(b) that the thrust ripple in the cascade-DTC method is less than the other two methods, correspondingly.

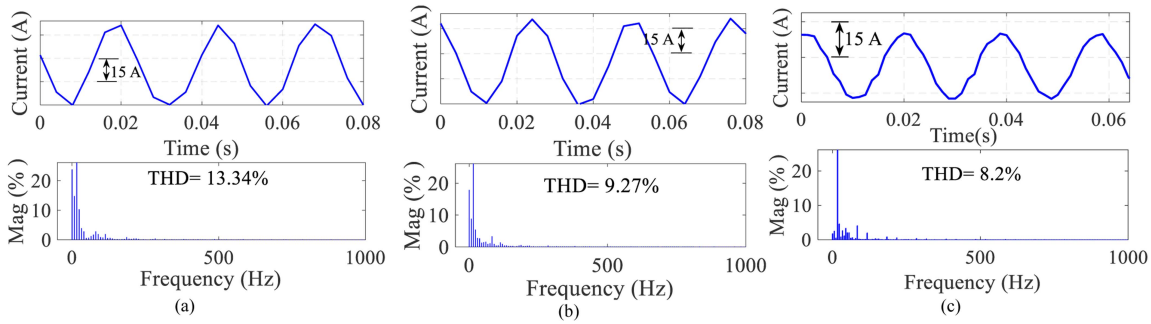

Fig. 19. Harmonic spectrum of the current response of the AIM under steady state condition. (a) CDTC. (b) FTSMC-DTC. (c) Cascade-DTC.

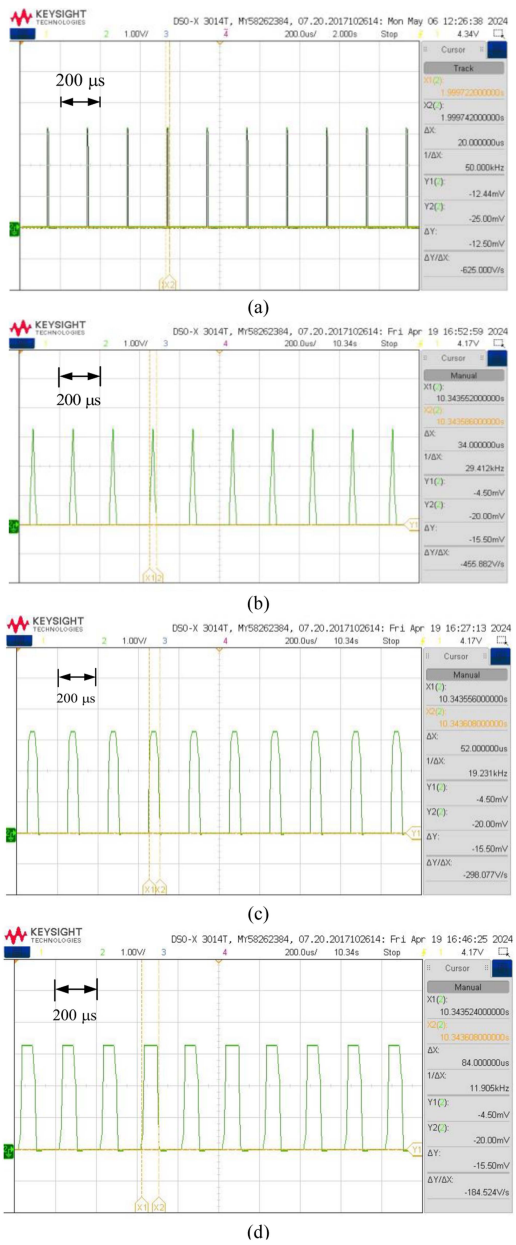

Fig. 20. Computation time response of the four control methods. (a) Conventional direct thrust control. (b) CSMC-DTC. (c) FTSMC-DTC. (d) Cascade-DTC.

TABLE VI
SPEED, THRUST, AND FLUX RIPPLE ANALYSIS UNDER CDTC, FTSM-DTC, AND CASCADE-DTC METHODS FOR THREE DIFFERENT CASES

Dynamic behaviors / Different states		CDTC	FTSMC-DTC	Cascade-DTC
Speed	Startup	1.24	1.11	1.05
	Speed variation	0.4	0.3	0.3
	Load change	0.35	0.19	0.19
Thrust	Startup	1.06	1.02	0.62
	Speed variation	1.06	1.02	0.62
	Load change	1.06	1.02	0.62
Flux	Startup	0.68	0.59	0.62
	Speed variation	0.69	0.57	0.61
	Load change	0.67	0.55	0.59

TABLE VII
PERFORMANCE ANALYSIS OF THE CDTC, FTSM-DTC, AND CASCADE-DTC METHODS FOR THREE DIFFERENT CASES

Method	CDTC	CSMC	FTSMC	Cascade
Transient response	Slow	Medium	Medium	Fast
Steady-state error	High	High	Low	Low
Thrust ripple	Low	High	Medium	Low
Flux ripple	High	High	Medium	Low
THD	High	High	Medium	Low
Computational burden	Low	Low	Medium	High

Fig. 24(a) shows the speed response under load change conditions. It can be noted from this figure that the cascade-DTC method has a quicker response with a better tracking error than CDTC-DTC and FTSMC-DTC, respectively. The flux behavior to the load change scenario is depicted in Fig. 24(c), which displays that the primary flux linkage has a significantly smaller flux ripple than CDTC, and FTSMC-DTC. The phase current of the LIM drive system under CDTC, CSMC-DTC, FTSMC-DTC, and cascade-DTC is displayed in Fig. 24(d) for load change conditions. The phase current is changing as load changes, but it is observed from the same figure that the peak value of the

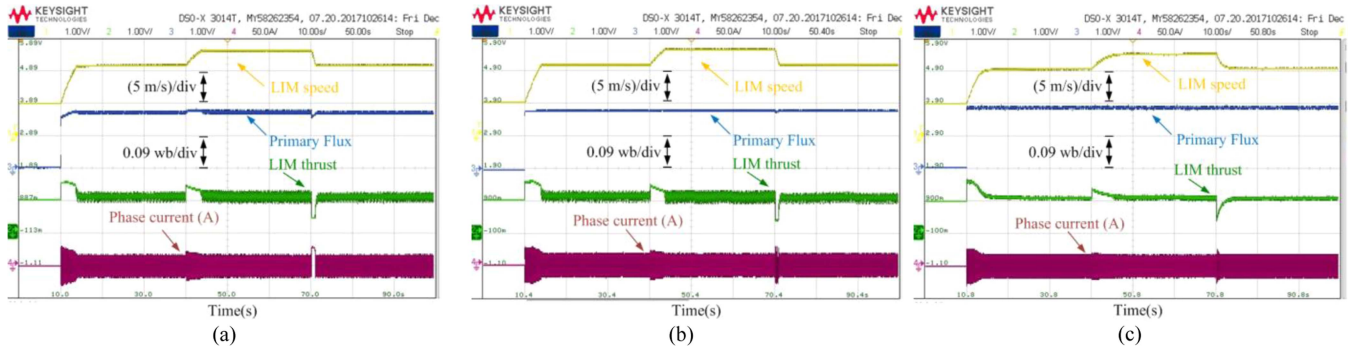

Fig. 21. The speed change profiles of the AIM under 100 N load with 6 to 8 m/s speed. (a) CDTC. (b) FTSMC-DTC. (c) Cascade-DTC.

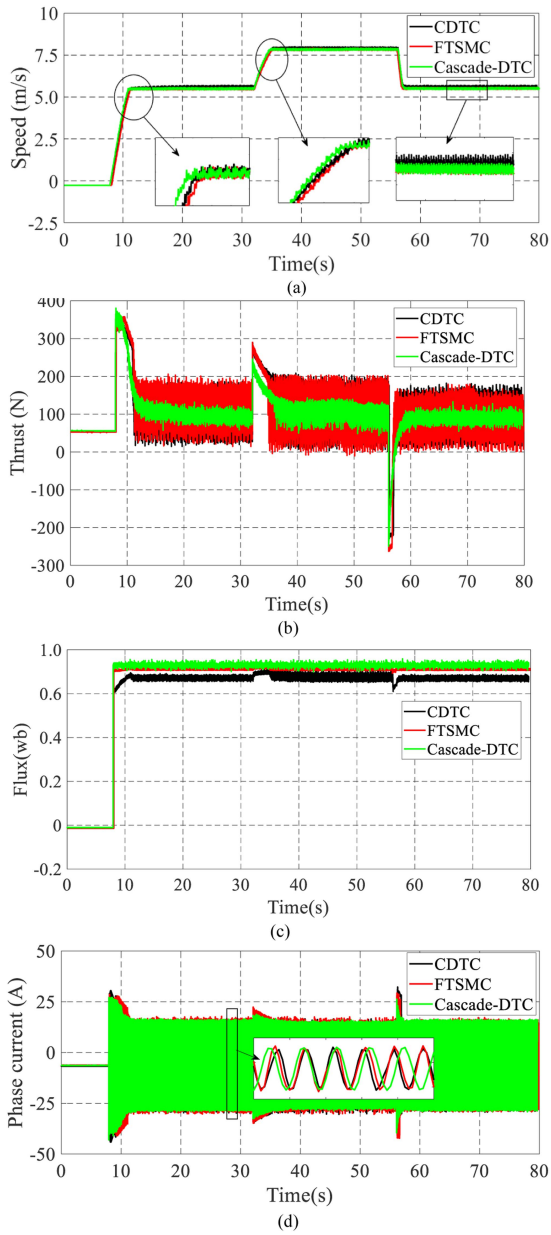

Fig. 22. Speed change performance of CDTC, FTSMC and cascade-DTC methods under 100 N load at 6 to 8 m/s and 8 to 6 m/s, respectively. (a) Speed. (b) Thrust. (c) Flux. (d) Phase current.

phase current is lesser with cascade-DTC than with CDTC, and FTSMC-DTC, finally.

Furthermore, the AIM has been started with a 150 N load with a constant speed of 6 m/s, then the load has been varied from 150 to 250 N, and again the load has been changed from 250 to 150 N under same speed for the three control methods. The thrust, linear speed, flux, and phase current responses of the LIM are shown in Fig. 25 under the load change scenario with 6 m/s speed, individually. It can be observed from the same picture that the thrust behavior under CDTC, FTSMC-DTC, and cascade-DTC tracks the reference thrust with constant speed. It can be further observed from Fig. 25(b) that the thrust ripple is lesser in the cascade-DTC method than FTSMC-DTC and CDTC, respectively. Fig. 25(a) shows the speed response under load change conditions. It can be noted from this figure that the cascade-DTC method has a quicker response with a better tracking error than CDTC-DTC and FTSMC-DTC, respectively.

The flux behavior to the load change scenario is depicted in Fig. 25(c), which shows that the primary flux linkage has a smaller flux ripple than the both methods. The phase current of the LIM drive system under CDTC, FTSMC-DTC, and cascade-DTC is displayed in Fig. 25(d) for load change conditions. The phase current is varying as load changes, but it is seen from the same figure that the peak value of the phase current is smaller with cascade-DTC than with CDTC, and FTSMC-DTC.

Moreover, Figs. 21 and 23 show the speed change and load change scenarios under the cascade-DTC, CDTC, and FTSMC-DTC methods. It can be seen from Figs. 21 and 23 that there are oscillations in speed response because of end effects and the complex friction dynamics of the AIM. Due to these oscillations in speed under three control methods, there is a ripple in the thrust and flux. But it can be seen from the same pictures that the proposed methods have a smaller thrust ripple than the CDTC and FTSMC-DTC, respectively.

The speed, thrust, and flux ripples of the CDTC, FTSMC-DTC, and cascade-DTC can be obtained through following expressions:

$$v_{(\text{ripple})}(\%) = \frac{\sqrt{\frac{1}{N}\sum_{i}^{N}\left(v_{(i)} - v_{\text{av}}\right)^2}}{v_{\text{av}}} \times 100 \tag{43}$$

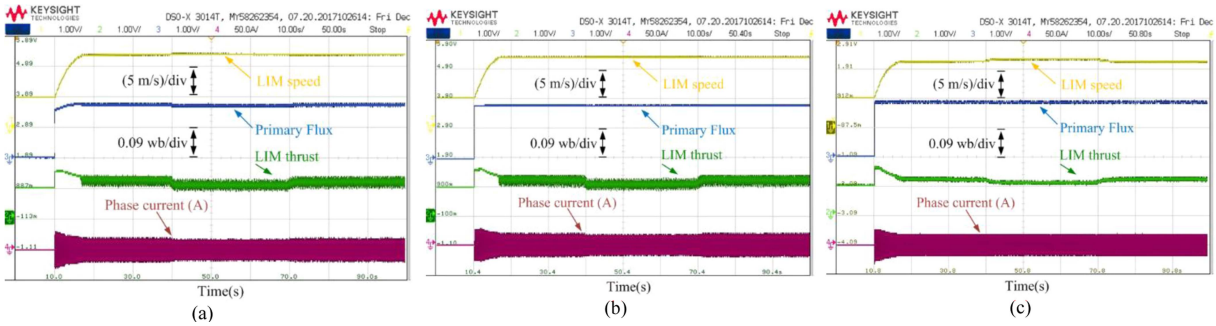

Fig. 23. The load change profiles of the AIM under 7 m/s speed with 150 N to 100 N load. (a) CDTC. (b) FTSMC-DTC. (c) Cascade-DTC.

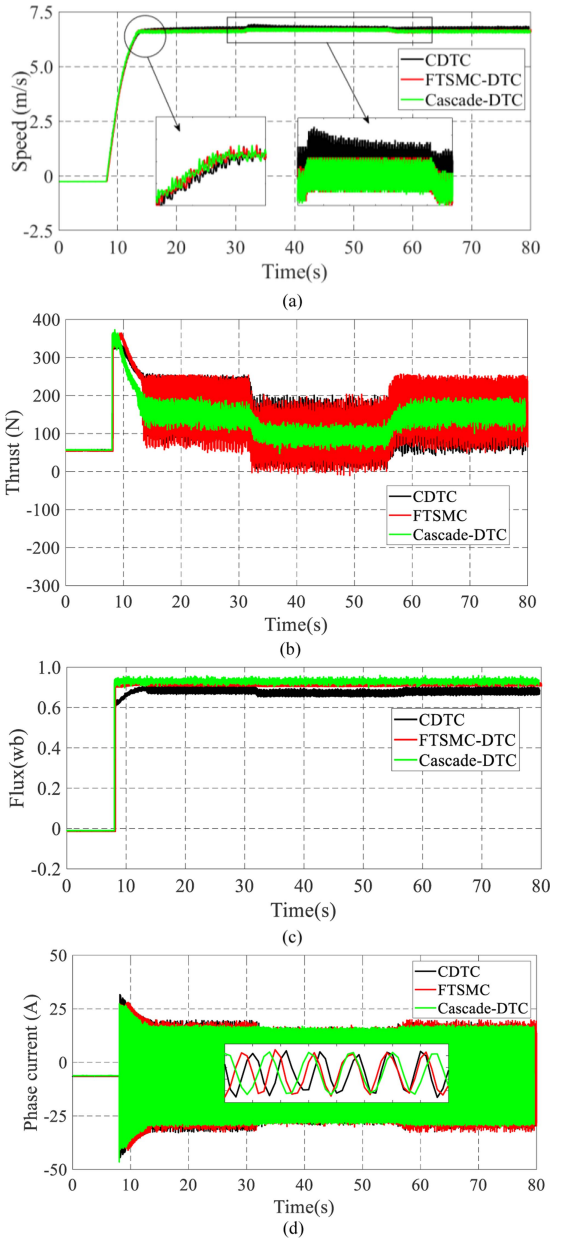

Fig. 24. Sudden load change performance of CDTC, FTSMC and cascade-DTC methods under 7 m/s at 300 to 50 N and 50 to 300 N, respectively. (a) Speed. (b) Thrust. (c) Flux. (d) Phase current.

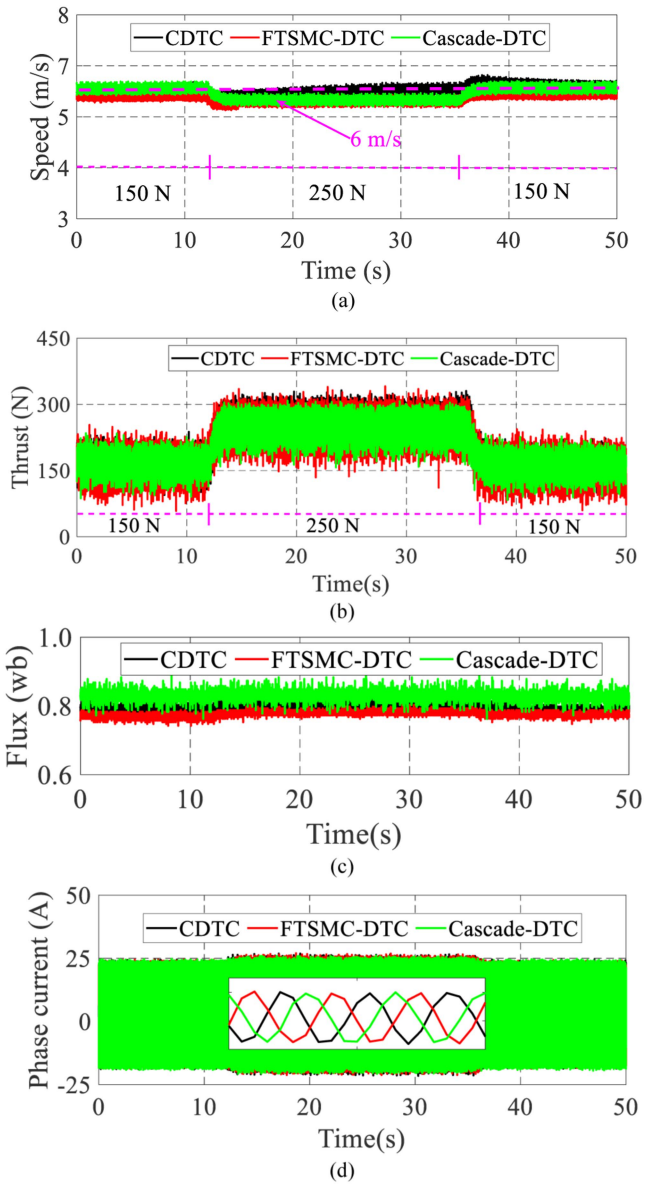

Fig. 25. Sudden load change performance of CDTC, FTSMC and cascade-DTC methods under 6 m/s at 150 to 250 N and 250 to 150 N, respectively. (a) Speed. (b) Thrust. (c) Flux. (d) Phase current.

$$F_{e(\text{ripple})}(\%) = \frac{\sqrt{\frac{1}{N}\sum_i^N \left(F_{(i)} - F_{\text{av}}\right)^2}}{F_{\text{av}}} \times 100 \quad (44)$$

$$\psi_{(\text{ripple})}(\%) = \frac{\sqrt{\frac{1}{N}\sum_i^N \left(\psi_{(i)} - \psi_{\text{av}}\right)^2}}{\psi_{\text{av}}} \times 100 \quad (45)$$

where N represents the total number of sampling points. It is observed from Table VI that the proposed method has advantages over the CDTC and FTSMC-DTC in terms of quick transient performance and lower thrust and flux ripples in all operating conditions. Furthermore, the comparative performance of the CDTC, CSMC, FTSMC, and proposed cascade method under three operating scenarios has been tested on AIM, which is given in Table VII. The superior performance of the propose method can be realized from Table VII than other three control methods, separately.

VII. Conclusion

In this article, a cascade sliding mode control based on DTC (cascade-DTC) is established to enhance the dynamic response of the LIM in a whole speed range. The summary of this article has been given below.

1) One cascade-DTC technique is established for the speed, thrust, and flux controllers to ensure fast dynamic performance, better tracking accuracy, strong steady state response, and a small thrust and primary flux ripples in the LIM. It can be observed from the simulation and experiments that the cascade-DTC method has a faster dynamic response with a smaller steady state error and a smaller thrust ripple than the CDTC and FTSMC-DTC, respectively. The decrease in thrust and flux ripples under cascade-DTC can reduce the noise and vibration of the LIM successfully.
2) It is verified from the experiments that the cascade-DTC method has a 4.84% and 0.77% smaller THD in the phase current than the CDTC and FTSMC-DTC, respectively.
3) The Lyapunov has been adopted to check the stability of the speed, thrust, and flux loop, respectively.
4) A comparative study is conducted over comprehensive simulation analysis among the CDTC, CSMC-DTC, FTSMC-DTC, and cascade-DTC methods, respectively. Moreover, the CDTC, FTSMC-DTC, and proposed (cascade-DTC) methods have been fully tested experimentally in three different operation scenarios.

It can be concluded from the simulation and experiments that the cascade-DTC method has superior response than the two other methods in terms of faster dynamic response, stronger robustness against load, and lower thrust and flux ripples, separately.

References

[1] I. Boldea, L. Tutelea, W. Xu, and M. Pucci, "Linear electric machines, drives and MAGLEVs: An overview," *IEEE Trans. Ind. Electron.*, vol. 65, no. 9, pp. 7504–7515, Sep. 2018.

[2] K. Wang, Y. Li, Q. Ge, and L. Shi, "An improved indirect field-oriented control scheme for linear induction motor traction drives," *IEEE Trans. Ind. Electron.*, vol. 65, no. 12, pp. 9928–9937, Dec. 2018.

[3] W. Xu, X. Xiao, G. Du, D. Hu, and J. Zou, "Comprehensive efficiency optimization of linear induction motors for urban transit," *IEEE Trans. Veh. Technol.*, vol. 69, no. 1, pp. 131–139, Jan. 2020.

[4] R. Dian, W. Xu, J. Zhu, D. Hu, and Y. Liu, "An improved speed sensorless control strategy for linear induction machines based on extended state observer for linear metro drives," *IEEE Trans. Veh. Technol.*, vol. 67, no. 10, pp. 9198–9210, Oct. 2018.

[5] J. Lim, D.-Y. Park, and J.-H. Jeong, "A study on optimal operating point of linear induction motor considering normal force and efficiency in MAGLEV vehicle," *IEEE Trans. Magn.*, vol. 54, no. 11, pp. 1–5, Nov. 2018.

[6] W. Xu et al., "Advanced methodologies on design and control for linear induction machine and drive adopted to urban transportation," *CES Trans. Elect. Machines Syst.*, vol. 6, no. 2, pp. 216–222, Jun. 2022.

[7] J. Ge, W. Xu, Y. Liu, F. Xiong, and D. Li, "Investigation on winding theory for short primary linear machines," *IEEE Trans. Veh. Technol.*, vol. 70, no. 8, pp. 7400–7412, Aug. 2021.

[8] W. Xu, Y. Tang, D. Dong, X. Xiao, E. Rashad, and A. K. Junejo, "Optimal reference primary flux based model predictive control of linear induction machine with MTPA and field-weakening operations for urban transit," *IEEE Trans. Ind. Appl.*, vol. 58, no. 4, pp. 4708–4721, Aug. 2022.

[9] C. Lascu, A. Argeseanu, and F. Blaabjerg, "Super-twisting sliding-mode direct torque and flux control of induction machine drives," *IEEE Trans. Power Electron.*, vol. 35, no. 5, pp. 5057–5065, May 2020.

[10] R.-J. Wai and C.-C. Chu, "Robust Petri fuzzy-neural-network control for linear induction motor drive," *IEEE Trans. Ind. Electron.*, vol. 54, no. 1, pp. 177–189, Feb. 2007.

[11] A. Berzoy, J. Rengifo, and O. Mohammed, "Fuzzy predictive DTC of induction machines with reduced torque ripple and high-performance operation," *IEEE Trans. Power Electron.*, vol. 33, no. 3, pp. 2580–2587, Mar. 2023.

[12] A. K. Junejo, W. Xu, C. Mu, M. M. Ismail, and Y. Liu, "Adaptive speed control of PMSM drive system based a new sliding-mode reaching law," *IEEE Trans. Power Electron.*, vol. 35, no. 11, pp. 12110–12121, Nov. 2020.

[13] W. Xu, A. K. Junejo, Y. Liu, M. G. Hussien, and J. Zhu, "An efficient anti-disturbance sliding-mode speed control method for PMSM drive systems," *IEEE Trans. Power Electron.*, vol. 36, no. 6, pp. 6879–6891, Jun. 2021.

[14] A. K. Junejo, W. Xu, F. F. M. El-Sousy, A. A. Hashmani, M. M. Ismail, and M. G. Hussien, "One new terminal reaching law based sliding mode with direct thrust control for the linear induction machines in metro transportation," *IEEE Energy Conv. Cong. Exp.*, 2022, pp. 1–6.

[15] W. Xu, M. M. Ali, M. F. Elmorshedy, S. M. Allam, and C. Mu, "One improved sliding mode DTC for linear induction machines based on linear metro," *IEEE Trans. Power Electron.*, vol. 36, no. 4, pp. 4560–4571, Apr. 2021.

[16] S.-K. Kim, J.-S. Lee, and K.-B. Lee, "Offset-free robust adaptive back-stepping speed control for uncertain permanent magnet synchronous motor," *IEEE Trans. Power Electron.*, vol. 31, no. 10, pp. 7065–7076, Oct. 2016.

[17] C. S. Lim, S. S. Lee, and E. Levi, "Continuous-control-set model predictive current control of asymmetrical six- phase drives considering system nonidealities," *IEEE Trans. Ind. Electron.*, vol. 70, no. 8, pp. 7615–7626, Aug. 2023.

[18] E. Quintero-Manriquez, E. N. Sanchez, R. G. Harley, S. Li, and R. A. Felix, "Neural inverse optimal control implementation for induction motors via rapid control prototyping," *IEEE Trans. Power Electron.*, vol. 34, no. 6, pp. 5981–5992, Jun. 2019.

[19] S. Lian et al., "Adaptive attitude control of a quadrotor using fast nonsingular terminal sliding mode," *IEEE Trans. Ind. Electron.*, vol. 69, no. 2, pp. 1597–1607, Feb. 2022.

[20] Y. Su, "Comments on 'A new adaptive sliding-mode control scheme for application to robot manipulators," *IEEE Trans. Ind. Electron.*, vol. 67, no. 8, pp. 7116–7120, Aug. 2020.

[21] S. Oucheriah and L. Guo, "PWM-based adaptive sliding-mode control for boost DC–DC converters," *IEEE Trans. Ind. Electron.*, vol. 60, no. 8, pp. 3291–3294, Aug. 2013.

[22] M. V. De Paula, S. S. Williamson, and T. A. .. S. Barros, "Four-quadrant model following sliding mode cruise control for SRM with DITC applied to transportation electrification," *IEEE Trans. Transport. Electrific.*, vol. 8, no. 3, pp. 3090–3099, Sep. 2022.

[23] F.-J. Lin and R.-J. Wai, "Robust control using neural network uncertainty observer for linear induction motor servo drive," *IEEE Trans. Power Electron.*, vol. 17, no. 2, pp. 241–254, Mar. 2002.

[24] Y. Kali, J. Rodas, M. Saad, R. Gregor, K. Benjelloun, and J. Doval-Gandoy, "Current control based on super-twisting algorithm with time delay estimation for a five-phase induction motor drive," in *Proc. IEEE Int. Elect. Mach. Drives Conf.*, 2017, pp. 1–8.
[25] M. Rasheed et al., "Sensorless second-order sliding-mode speed control of a voltage-feed induction-motor drive using nonlinear state feedback," *IEEE Proc. Elect. Power Appl.*, vol. 152, no. 5, pp. 1127–1136, Sep. 2005.
[26] L. Zhao, J. Huang, H. Liu, B. Li, and W. Kong, "Second-order sliding-mode observer with online parameter identification for sensorless induction motor drives," *IEEE Trans. Ind. Electron*, vol. 61, no. 10, pp. 5280–5289, Oct. 2014.
[27] C. Lascu, A. Argeseanu, and F. Blaabjerg, "Super twisting sliding-mode direct torque and flux control of induction machine drives," *IEEE Trans. Power Electron*, vol. 35, no. 5, pp. 5057–5065, May 2020.
[28] A. Levant, "Sliding order and sliding accuracy in sliding mode control," *Int. J. Control*, vol. 58, no. 6, pp. 1247–1263, Dec. 1993.
[29] W. Xu, R. Islam, and M. Pucci, *Advanced Linear Machines and Drive Systems*, Berlin, Germany: Springer, Aug. 2019.
[30] R. Seeber, M. Horn, and L. Fridman, "A novel method to estimate the reaching time of the super-twisting algorithm," *IEEE Trans. Autom. Control*, vol. 63, no. 12, pp. 4301–4308, Dec. 2018.
[31] W. Xu, A. K. Junejo, Y. Liu, and M. R. Islam, "Improved continuous fast terminal sliding mode control with extended state observer for speed regulation of PMSM drive system," *IEEE Trans. Veh. Technol.*, vol. 68, no. 11, pp. 10465–10476, Nov. 2019.
[32] M. M. Ali, W. Xu, A. K. Junejo, M. F. Elmorshedy, and Y. Tang, "One new super-twisting sliding mode direct thrust control for linear induction machine based on linear metro," *IEEE Trans. Power Electron.*, vol. 37, no. 1, pp. 795–805, Jan. 2022.
[33] R. Seeber, M. Horn, and L. Fridman, "A novel method to estimate the reaching time of the super-twisting algorithm," *IEEE Trans. Autom. Control*, vol. 63, no. 12, pp. 4301–4308, Dec. 2018.
[34] A. K. Junejo et al., "Novel sliding mode reaching law based on DTC for linear induction machine applied to linear Metro," *IEEE Trans. Transport. Electrific.*, to be published, doi: 10.1109/TTE.2023.3340343..

Abdul Khalique Junejo (Senior Member, IEEE) received the B.E. and M.E. degrees in electrical engineering from Quaid-e-Awam UEST Nawabshah, Sindh, Pakistan, in 2011 and 2015, respectively, and the Ph.D. degree in electrical engineering with the School of Electrical and Electronics Engineering, State Key Laboratory of advanced Electromagnetic Engineering, Huazhong University of Science and Technology, Wuhan, China.

He is currently a Postdoc Fellow with the School of Electrical and Electronics Engineering, Huazhong University of Science and Technology, Wuhan, China. He is also an Assistant Professor with Quaid-e-Awam UEST Nawabshah, Sindh, Pakistan. He has authored or coauthored 22 SCI Journal papers including 15 IEEE papers (IEEE TRANSACTIONS ON VEHICULAR TECHNOLOGY, IEEE TRANSACTIONS ON POWER ELECTRONICS, IEE-TTE IEEE-EC, IEEE INDUSTRY APPLICATIONS SOCIETY, and IEEE ACCESS), 2 others, 1 ESCI and 15 national and international journals, respectively. Furthermore, he attended and published international conferences on machines including ICEMS, LIDA and ECCE separately. His research interests include the sliding mode control, direct torque control, model predictive control and sensorless control methods for permanent magnet synchronous machines, Induction machines, linear IM and drives and renewable energies.

Dr. Junejo was a Reviewer for IEEE journals (including IEEE TRANSACTIONS ON INDUSTRIAL ELECTRONICS, IEEE TRANSACTIONS ON POWER ELECTRONICS, and IEEE TRANSACTIONS ON TRANSPORTATION ELECTRIFICATION, IEEE TRANSACTIONS ON INDUSTRY APPLICATION SOCIETY, IEEE TRANSACTIONS ON MECHATRONICS, *Article in Journal* and IEEE JOURNAL OF EMERGING AND SELECTED TOPICS IN INDUSTRIAL ELECTRONICS and Emerald Group Publishing Ltd. Assembly Automation). His paper has been selected as one of the best papers published during 2019–2020 in IEEE TRANSACTIONS ON ENERGY CONVERSION IN THE POWER GENERATIONS SYSTEMS AND GRID INTERFACES AREA.

Wei Xu (Fellow IEEE, 2024) received the double B.E. and M.E. degrees from Tianjin University, Tianjin, China, in 2002 and 2005, and the Ph.D. degree from the Institute of Electrical Engineering, Chinese Academy of Sciences (IEECAS), Xi'an, China, in 2008, all in electrical engineering.

His research topics mainly focus on design and control for linear machines and drives. From 2008 to 2012, he was a Postdoctoral Fellow with the University of Technology Sydney, the Vice Chancellor Research Fellow with Royal Melbourne Institute of Technology, Japan Science Promotion Society Invitation Fellow with Meiji University, respectively. From 2013 to 2023, he was one Professor with Huazhong University of Science and Technology, China. Since 2024, he has been one Professor with IEECAS.

Dr. Xu is a Fellow of the Institute of Engineering and Technology. He is the General Chair for 2021 International Symposium on Linear Drives for Industry Applications and 2023 IEEE International Conference on Predictive Control of Electrical Drives and Power Electronics. He has been an Associate Editor for ten peer-review IEEE journals, including IEEE TRANSACTIONS ON INDUSTRIAL ELECTRONICS, IEEE TRANSACTIONS ON POWER ELECTRONICS, and so on.

Yirong Tang (Student Member, IEEE) received the B.E. degree in electrical engineering in 2020. from the Huazhong University of Science and Technology, Wuhan, China, where he is currently working toward the Ph. D. degree with the State Key Laboratory of Advanced Electromagnetic Engineering and Technology.

His research interests include advanced control methods for permanent magnet synchronous machines, linear induction machines and drives.

Kaiju Liao was born in Linyi, China. He received the B.E. degree in automation from the Shandong University of Technology, Zibo, China, in 2017, and the M.E. degree in control engineering from Tianjin University, Tianjin, China, in 2020. He is currently working toward the Ph.D. degree in electrical engineering with the State Key Laboratory of Advanced Electromagnetic Engineering and Technology, Huazhong University of Science and Technology, Wuhan, China.

His research interests include position sensorless control and resonant frequency tracking control for linear compressor.

Han Xiao was born in Henan, China. He received the B.S. and M.S. degrees in electrical engineering and automation from Zhengzhou University of Light Industry, Zhengzhou, China, in 2019 and 2022, respectively. He is currently working toward the Ph.D. degree in electrical engineering with the Huazhong University of Science and Technology.

His research interests include model predictive control for linear induction machines and power converters.

Yaohua Li (Member, IEEE) was born in Henan, China, in 1966. He received the Ph.D. degree in power electronics and power drives from Tsinghua University, Beijing, China, in 1994.

From 1995 to 1997, he was a Postdoctoral Research Fellow with the Institute of Electrical Machines, Technical University of Berlin, Berlin, Germany. In 1997, he was with the Institute of Electrical Engineering, Chinese Academy of Sciences, Beijing, China, where he is currently a Professor and the Director. His current research interests include the analysis and control of electrical machines and power electronics.